Soft Matter

PAPER

View Article Online
View Journal | View Issue

Cite this: Soft Matter, 2015, 11, 6318

Enhancing thermal stability and mechanical properties of lyotropic liquid crystals through incorporation of a polymerizable surfactant

Shuhua Peng,[ab] Patrick G. Hartley,*[b] Timothy C. Hughes*[b] and Qipeng Guo*[a]

Received 6th July 2015,
Accepted 6th July 2015

DOI: 10.1039/c5sm01646k

www.rsc.org/softmatter

We present a facile method to prepare thermally stable and mechanically robust crosslinked lyotropic liquid crystals (LLCs) through incorporation of a polymerizable amphiphile into a binary LLC system comprising commercially available surfactant Brij 97 and water. Thermal stability and mechanical properties of the polymerized LLCs were significantly enhanced after polymerization of the incorporated polymerizable surfactant. The effect of incorporating a polymerizable amphiphile on the phase behavior of the LLC system was studied in detail. In situ photo-rheology was used to monitor the change in the mechanical properties of the LLCs, namely the storage modulus, loss modulus, and viscosity, upon polymerization. The retention of the LLC nanostructures was evaluated by small angle X-ray scattering (SAXS). The ability to control the thermal stability and mechanical strength of LLCs simply by adding a polymerizable amphiphile, without tedious organic synthesis or harsh polymerization conditions, could prove highly advantageous in the preparation of robust nanomaterials with well-defined periodic structures.

Introduction

As one of the most common self-assembled systems, lyotropic liquid crystals (LLCs) are ubiquitous in nature and they have immediate relevance in biology due to the self-organized biological bilayer membranes in living systems.[1] LLCs often exhibit the low viscosity characteristic of fluids while maintaining a highly ordered morphology more typical of solid materials.[2] LLCs prepared by self-assembly of amphiphillic surfactants and lipids have been widely employed to synthesize interesting nanostructured materials with controllable structures and properties.[1–7] A variety of LLC phases, i.e., cubic, lamellar, and hexagonal, can be formed depending on the concentration and nature of the surfactants and solvent. The geometric diversity of these LLC mesophases has the potential to prepare a variety of nanomaterials with different architectures.[8–11] Aside from their use as templates for the synthesis of mesoporous inorganic materials,[12,13] LLCs have received much attention because of their potential applications in biological studies, such as the capture and replication of viruses,[14] drug delivery,[15–17] medical imaging,[18,19] and protein crystallisation.[20–22]

However, the lack of thermal stability and mechanical strength has greatly limited the use of LLCs in materials applications where mechanically durable and thermally stable structures are required. Polymerizable or cross-linkable LLCs provide a feasible solution to this problem.[1] The resulting covalently crosslinked LLCs with robust networks have been used for controlled particle synthesis,[23] drug delivery agents,[24] heterogeneous catalysis and separations,[6] and templates for nanocomposites and anisotropic metallization.[25,26] Although the use of polymerizable LLCs has been demonstrated, an effective method to improve the mechanical strength and thermal stability of their precursors and retention of the parent LLC nanostructure throughout the polymerization reaction can be challenging.[5,27,28] Thermodynamically driven phase separation events often occur during polymerization, leading to polymer networks with larger and more disordered structures than the original LLC templates. Efforts to elucidate the factors including initiation rate, photoinitiator mobility, reaction speed, temperature, monomer segregation behavior, and variations in polymerization rate have been extensively investigated to provide considerable control over the final state of polymerized LLCs structures by manipulating environment during the polymerization reaction.[2,4–7,27–36]

It was reported by Gin et al. that the order of the original LLC template can be largely retained when polymerizable amphiphiles (i.e., surfactants) were employed as the LLC mesogens.[37–39] Catalytic functional groups were incorporated into these polymerizable amphiphiles and the crosslinked LLC assemblies with well-defined nano-channels and/or pores have been successfully applied for heterogeneous catalysis and selective separation.[6] However, the design and synthesis of these polymerizable

[a] Polymers Research Group, Institute for Frontier Materials, Deakin University, Locked Bag 20000, Geelong, Victoria 3220, Australia. E-mail: qguo@deakin.edu.au
[b] CSIRO Materials Science and Engineering, Bayview Avenue, Clayton South, Victoria 3169, Australia. E-mail: patrick.hartley@csiro.au, tim.hughes@csiro.au

amphiphilic monomers requires careful consideration of their mesogenic behavior, amphiphilic self-assembly, and polymerization activity, which makes these polymerizable LLCs scarcely accessible. Thus, there is a need for new polymerizable LLCs with the capability of full retention of their parent nanostructures that could be easily prepared from existing chemicals and/or simple organic synthesis.

In this work, a simple polymerizable LLC system based on a combination of polymerizable amphiphile and nonpolymerizable surfactants was developed to prepare polymerized LLCs with enhanced thermal stability and mechanical strength. The newly designed and synthesized siloxane macromonomer, from a one-step reaction, is an amphiphile that forms part of the polymerizable LLC system. Real-time photo-rheology measurements were performed to follow the dynamic changes of moduli and viscosity during the course of LLC polymerization. The elastic and viscous moduli of polymerized LLCs were quantitatively evaluated at a constant strain rate as a function of UV exposure time. The structures of LLCs were investigated before and after polymerization to determine the retention of the parent LLC nanostructures. In addition, the thermal stability of the polymerized LLCs located in different phase regions was also demonstrated.

Experimental section

Materials

Triblock copolymer poly(ethylene oxide)-block-polydimethylsiloxane-block-poly(ethylene oxide) (PEO–PDMS–PEO, DBE-C25, M_w = 3500–4500, 60 wt% non-siloxane) was purchased from Gelest and was dried using 4 Å molecular sieves for at least 24 h before use. 2-Isocyanatoethyl methacrylate (IEM), purchased from Amtrade International Pty. Ltd, was purified by distillation under reduced pressure, and stored in a closed vessel under dark condition at −20 °C prior to use. Dibutyltin dilaurate (DBTDL) was obtained from Merck Co; surfactant Brij 97 and photoinitiator (2-hydroxy-2-methylpropiophenone, 97%) supplied by Sigma-Aldrich were used as received.

Synthesis of polymerizable PEO–PDMS–PEO dimethacrylate

Polymerizable PEO–PDMS–PEO dimethacrylate (MA–PEO–PDMS–PEO–MA) was prepared by a similar method reported in our previous work[32] and the synthesis route is shown in Scheme 1. Briefly, hydroxyl-terminated PEO–PDMS–PEO (12.0 g, 0.012 mol) and IEM (4.0 g, 0.026 mol) were added into a round-bottom flask fitted with a Teflon-coated magnetic stirrer bar. The flask was sealed and stirred vigorously to produce a homogeneous solution. After 10 min, the catalyst DBTDL (20 mL) was added into the flask and the solution was stirred for 24 h to ensure a complete reaction in the absence of light at room temperature. Proton nuclear magnetic resonance (^{1}H NMR) spectra of MA–PEO–PDMS–PEO–MA were recorded on a Bruker NMR spectrometer at 400 MHz using deuterated chloroform as the solvent. ^{1}H NMR chemical shifts (δ) in parts per millions (ppm) were referenced relative to chloroform (δ = 7.26 ppm) as an internal standard.

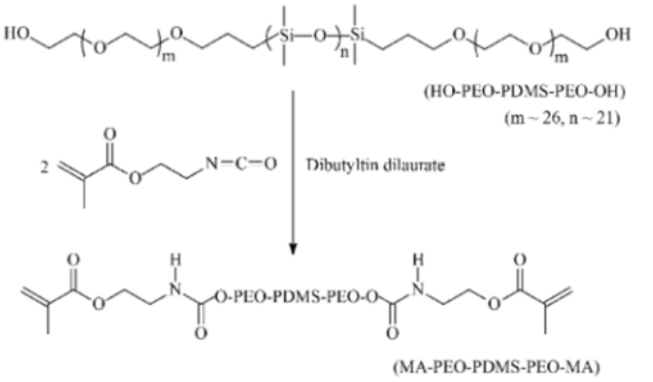

Scheme 1 Synthesis route of polymerizable amphiphile MA–PEO–PDMS–PEO–MA.

Polarised optical microscopy (POM)

Birefringent textures were observed with a Nikon Eclipse 80i cross-polarised optical microscope equipped with a Linkam hot stage and controller (LTS 120 with PE94 controller, Linkam UK). Images were captured with a Nikon Ds-Fi1 CCD camera equipped with DS-U2 controller (Nikon Australia Pty. Ltd., Melbourne, Australia).

Small angle X-ray scattering (SAXS)

SAXS experiments were performed at the Australian Synchrotron on the small/wide angle X-ray scattering beamline as previously described.[31,40] Briefly, samples were inserted into 1.0 mm glass capillaries which were then sealed. The background correction was performed by measuring the scattering of an empty capillary and correcting for sample absorption. Asliver behenate was used to calibrate the sample to detector distance. Data reduction (calibration and integration) of data collected using a 2D detector was achieved using AXcess, a custom-written SAXS analysis program written by Dr Andrew Heron from Imperial College, London.[41]

Determination of phase diagram

The partial ternary phase diagram of Brij 97/water/MA–PEO–PDMS–PEO–MA mixture system at room temperature was determined by combination of SAXS and POM. In order to prepare the systems of varying compositions, different ratios of Brij 97 and MA–PEO–PDMS–PEO–MA were prepared firstly and then the required amount of water was added to the mixture of Brij 97 and MA–PEO–PDMS–PEO–MA. The ternary mixtures were thoroughly mixed using a Vortex mixer after they were gently heated above the phase-separation temperature where the mixtures exhibited a rather low viscosity.[42] After that, they were sonicated and centrifuged repeatedly until homogeneous samples were obtained. Lyotropic phase region of the ternary system was identified by both POM and SAXS with a concentration accuracy of 5 wt% water content.

Polymerization of LLCs by UV

LLCs formulations were polymerized using 1 wt% photoinitiator (2-hydroxy-2-methylpropiophenone, 97%), which was based on the weight of polymerizable MA–PEO–PDMS–PEO–MA.

The fresh LLCs were firstly loaded into 1.0 mm borosilicate glass capillaries and then the sealed capillaries were put into the UV box for polymerization. Photo-polymerization was carried out in a UV box working at a wavelength of 365 nm (with an output of 10 mW cm^{-2}) for about 30 min at room temperature.

In situ monitoring of polymerization of LLCs by photo-rheology

In situ monitoring of the UV curing process for polymerization of LLC phases was conducted using an ARES photo-rheometer (TA Instruments, USA) connected to an EXFO Acticure 4000 light source working at 100 mW cm^{-2} (365 nm). A Peltier temperature controller was also connected to the rheometer to maintain the cure temperature at 25 1C, thereby ensuring that both rheological and SAXS experiments were performed under the same conditions for phase behaviour study. A description of these fixtures is given in our previous work.[9,32] The samples were loaded in the centre of two parallel plates of 20 mm in diameter. The gap between the two plates was set at 0.3 mm. The in situ cure kinetics was studied at a constant temperature of 25 1C for 10 min. For the first 2 min, the light source was controlled in off-mode to get a baseline and automatically converted to on-mode for 18 min. Storage shear modulus (G'), the loss shear modulus (G''), and complex viscosity ($|\eta^*|$) were measured as a function of time at a constant frequency of 100 rad s^{-1} and a strain of 1.0%.

Results and discussion

Characterization of MA–PEO–PDMS–PEO–MA

The ^{1}H NMR spectra of HO–PEO–PDMS–PEO–OH and MA–PEO–PDMS–PEO–MA are respectively shown in Fig. 1. Conversion of HO–PEO–PDMS–PEO–OH to MA–PEO–PDMS–PEO–MA was evidenced by the upfield shift of proton signals from methylene next to OH group. All the peaks were assigned and the integral ratios of the peaks matched the assigned structure, demonstrating that polymerizable MA–PEO–PDMS–PEO–MA was successfully synthesized.

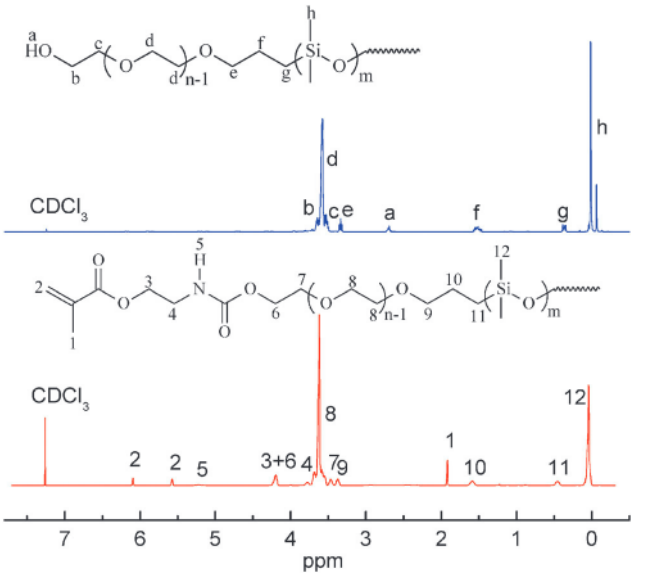

Fig. 1 ^{1}H NMR spectra of HO–PEO–PDMS–PEO–OH and MA–PEO–PDMS–PEO–MA in $CDCl_3$.

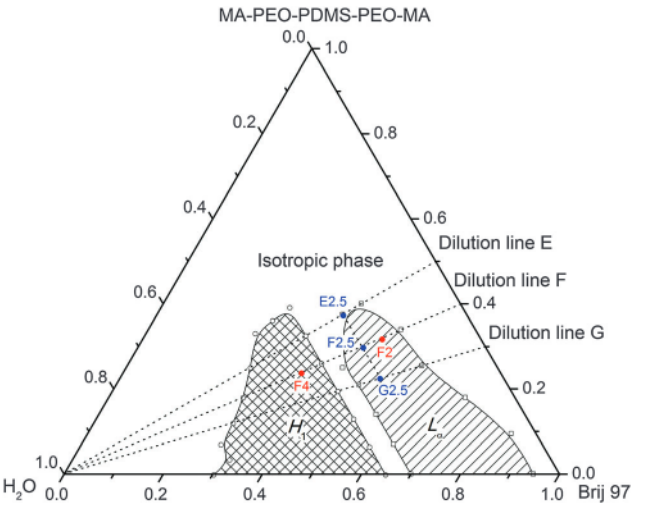

Fig. 2 Partial lyotropic phase behaviour of the Brij 97/water/MA–PEO–PDMS–PEO–MA at room temperature. Three water dilution lines E, F, and G were indicated. Three formulations with constant water contents (25 wt%, E25, F25, and G25) and three formulations with increasing water content (F20, F25, and F40) along dilution line F were indicated for the following mechanical and thermal stability study.

Phase diagram of the Brij 97/Water/MA–PEO–PDMS–PEO–MA

On the basis of visual inspection, POM, and SAXS analysis of around 120 samples, the isotropic phase and lyotropic phase for the Brij 97/water/MA–PEO–PDMS–PEO–MA ternary system have been identified. An approximate partial phase diagram, determined at 25 1C, is illustrated in Fig. 2. It mainly exhibits two lyotropic mesophases: lamellar phase L_a and normal hexagonal phase H_1. The phase boundary of these lyotropic phases was established with an accuracy of 5 wt% water content. As shown in Fig. 2, it can be clearly seen that these lyotropic phases are close to the high Brij 97 content region. This is presumably due to the templating effect of Brij 97. There have been extensive studies using Brij 97 as a template for the synthesis of mesoporous inorganic materials.[43,44] The polymerizable MA–PEO–PDMS–PEO–MA with 60 wt% hydrophilic blocks cannot self-assemble into well-defined LLCs because of its good water solubility. However, with an appropriate ratio of Brij 97, the mixture of Brij 97/MA–PEO–PDMS–PEO–MA exhibits the ability to form lyotropic mesophases. Two large lyotropic phase regions were observed for the Brij 97/water/MA–PEO–PDMS–PEO–MA ternary system in Fig. 2.

A water dilution line which went through both lamellar and hexagonal phases was selected for the following polymerization study due to the relatively high polymerizable MA–PEO–PDSM–PEO–MA content (dilution line F, Fig. 2). As shown in Fig. 3, the formulations along dilution line F in the lyotropic regions exhibited brightness between crossed polarized films because of their anisotropic characteristics. In contrast, for the formulations with 10 wt% and 60 wt% water corresponded to the isotropic and

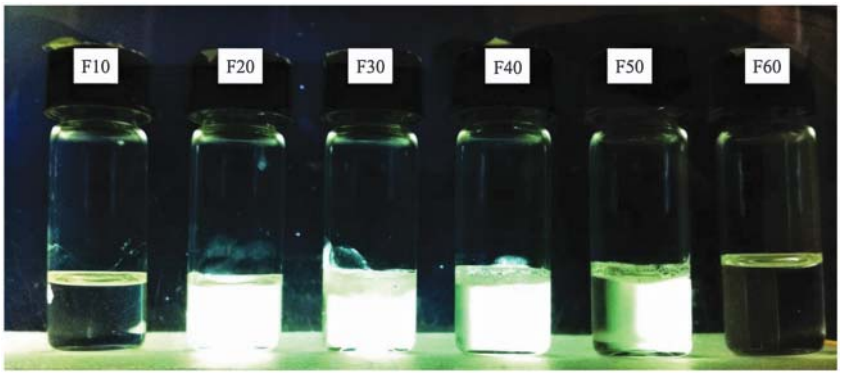

Fig. 3 Samples along water dilution line F with different water contents were observed between cross polarized films.

non-birefringent phases did not show brightness under cross polarized light. Meanwhile, two representative POM optical textures for the Brij 97/water/MA–PEO–PDMS–PEO–MA ternary system with 20 wt% and 40 wt% water were presented in Fig. 4, respectively. Characteristic streaked texture for lamellar phase was observed for the ternary system with 20 wt% water content. The ternary mixture with 40 wt% water showed a typical parallel striation texture consistent with the formation of a hexagonal phase.[42]

SAXS measurements were further used to identify different LLC mesophases based on the characteristic diffraction pattern of the Bragg peaks.[43] Specifically, the relative peak positions for a lamellar phase (L_a) are 1 : 2 : 3 : 4 and for a hexagonal phase are 1 : 0 3 : 0 4 : 0 7. As shown in Fig. 5, a broad SAXS peak was observed for the formulation along water dilution line F with 15 wt% water. Meanwhile, lack of birefringence under crossed polarizers and low viscosity together suggested the presence of reverse micelles for the Brij 97/water/MA–PEO–PDMS–PEO–MA ternary mixture. With increasing water content to 20 wt%, the mixture evolved to lamellar phase, evidencing by the existence of two sharp SAXS peaks with relative positions 1 : 2. As the water content was increased to 30 wt%, these SAXS peaks became much broader and expressed the onset of phase transition. Three well developed SAXS peaks with the relative positions of 1 : 0 3 : 0 4 were observed when the water content reached to 40 wt% and 50 wt%, which is characteristic of well-defined hexagonal structures. Moreover, analysis of these SAXS patterns revealed that the lattice parameter increased from 6.23 nm to 6.79 nm as the water content was increased from 40 wt% to 50 wt%. The increase of lattice parameter seems to be due to the swelling effect of the normal hexagonal (H_1) phase by increasing water content.[9,43] With further increase of water content to 60 wt%, the ternary mixture transformed to the isotropic phase with broad SAXS peaks.

Real-time photo-rheology measurement during polymerization

Real-time photo-rheology measurements were performed to follow the LLC polymerization process. Elastic and viscous moduli of polymerizing LLCs were quantitatively evaluated when they were plotted as a function of UV exposure time at a constant frequency. In this study, the macromonomer (MA–PEO–PDMS–PEO–MA) formulations were cross-linked by exposing LLC formulations to UV light. As shown in Fig. 6, the dynamic changes of storage modulus (G^0), loss modulus (G^{00}), and viscosity (Z^*) with cure time were clearly observed for the lamellar phase with 25 wt% water content along the water dilution line F (Fig. 2) during the course of polymerization. The initial exposure of the mixture to UV light was intentionally delayed for 2 min to obtain a baseline for the measurement of the rheological properties. No change in moduli and viscosity was observed before the mixture was exposed to UV light. Upon exposure to UV light a fast increase of moduli and viscosity of the polymerizing LLC was observed and the plateau values were reached within 15 min. Two orders of magnitude increase of storage modulus (G^0) and viscosity (Z^*)

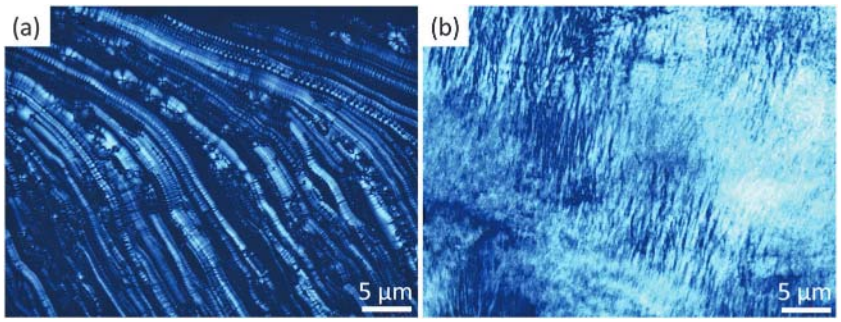

Fig. 4 Representative POM optical textures for the Brij 97/water/MA–PEO–PDMS–PEO–MA ternary system along water dilution line F with different water contents: (a) F20; (b) F40.

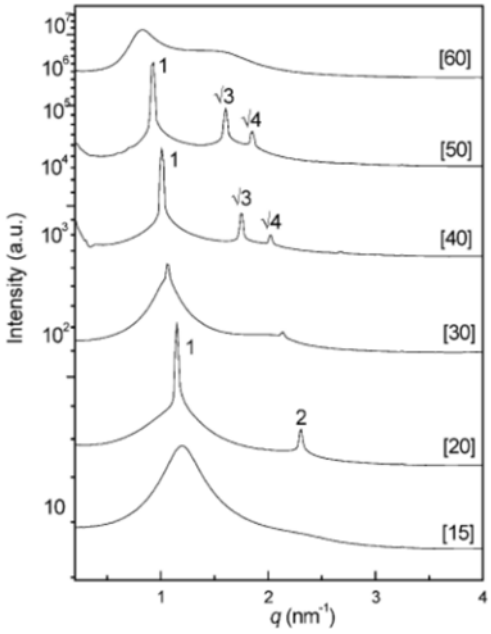

Fig. 5 SAXS patterns for the formulations along dilution line F and water contents are indicated in square brackets.

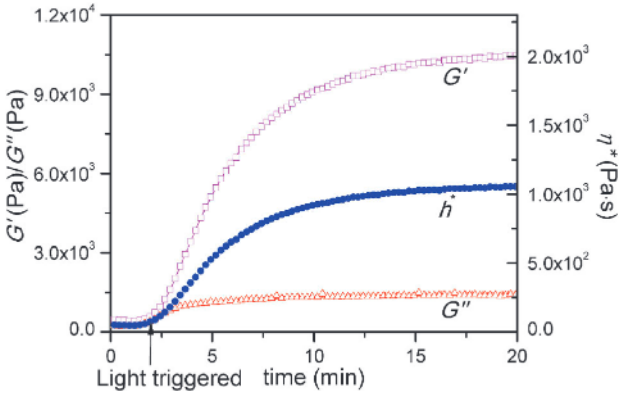

Fig. 6 Photo-rheology profile of cure process for a lamellar phase having 25 wt% water, 30 wt% MA–PEO–PDMS–PEO–MA, and 45 wt% Brij 97 (F25 in Fig. 2) following dilution line F.

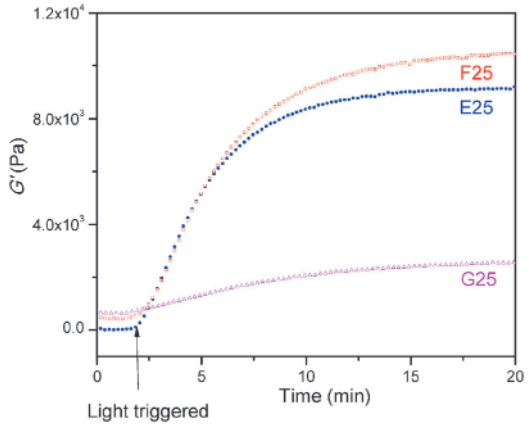

Fig. 7 Storage modulus (G^0) for the lamellar phases with constant water content (25 wt%) and variable polymerizable MA–PEO–PDMS–PEO–MA contents (E25, 37.5 wt%; F25, 30 wt%; G25, 22.5 wt%) and Brij 97 contents (E25, 37.5 wt%; F25, 45 wt%; G25, 52.5 wt%) during polymerization. The compositions of these lamellar phases are indicated in Fig. 2.

were observed after polymerization. The increase of moduli and viscosity was presumably due to the cross-linking of polymerizable MA–PEO–PDMS–PEO–MA. Meanwhile, Fig. 7 illustrates how the mechanical properties of the polymerized LLCs were affected by their corresponding precursor LLC phase behaviour. A series of polymerizable lamellar phases (E25, F25, and G25 in Fig. 2) with constant water content (25 wt%) and variable MA–PEO–PDMS–PEO–MA contents were selected for this study. As shown in Fig. 7, decreasing polymerizable MA–PEO–PDMS–PEO–MA content from 30 wt% (F25) to 22.5 wt% (G25) resulted in the reduced density of cross-links of the polymerized LLCs and a corresponding decrease of G^0 for G2.5 was observed.[45] It should be noted that, however, a lower plateau value of G^0 for the lamellar phase with higher polymerizable MA–PEO–PDMS–PEO–MA content (E25, 37.5 wt%) was recorded in Fig. 7. This may be due to the intrinsic structural characteristic of this lamellar phase (E25). The bilayer lamellar nanostructure of E25 was not likely to be well-developed because it was located near the phase boundary between lyotropic lamellar and isotropic micellar phase (Fig. 2). In addition, as shown in Fig. 7, a rather low initial G^0 value for E25 (compared with that of F25 and G25) was observed before polymerization, underscoring the intermediate phase behaviour of E25. Therefore, lack of well-developed bilayer lamellar structure for E25 resulted in a lower G^0 after polymerization even there was higher polymerizable content in its corresponding precursor LLC phase. Importantly, it also should be noted that initial lamellar and hexagonal phases were retained after polymerization (details will be given in the following section) and the increasing G^0 was merely due to the cross-linking of the polymerizable MA–PEO–PDMS–PEO–MA.

The effect of polymerization on the mechanical property of polymerizable LLCs in terms of shear storage modulus G^0 within different mesophase regions was summarized in Fig. 8. Generally, it can be clearly seen that G^0 increased at least one order of magnitude for all the LLC samples upon polymerization. More than three orders of magnitude increase of G^0 was observed for the lamellar phase with high polymerizable MA–PEO–PDMS–PEO–MA content (E25, 37.5 wt%). As for the polymerizable hexagonal phases, it should be noted that the initial G^0 was much higher than that of lamellar phases due to their highly ordered structures with array of long parallel cylinders.[9] Polymerization within hexagonal phases results in around one order of magnitude increase of G^0. The effect of polymerization on the mechanical property of polymerized LLCs with different mesophases was closely correlated with polymerizable surfactant content and intrinsic architecture of LLC mesophase. Compared with lamellar phase, hexagonal phase has higher surface area and hence the number of cross-linkers per surfactant surface is also higher. Further results and discussion about the effect of polymerization on the thermal stability of polymerized LLCs are given the following section.

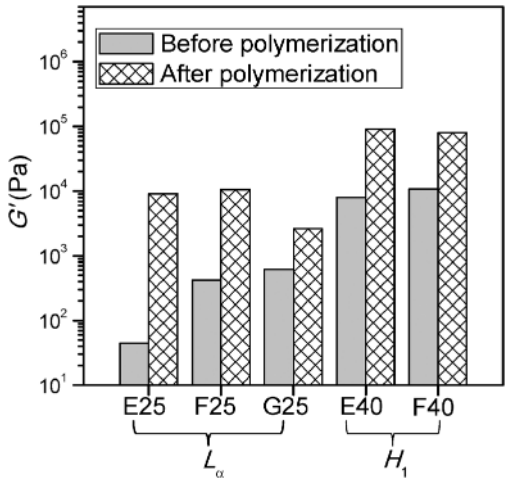

Fig. 8 Storage modulus (G^0) for the lamellar phases with 25 wt% water content and hexagonal phases with 40 wt% water content before and after polymerization.

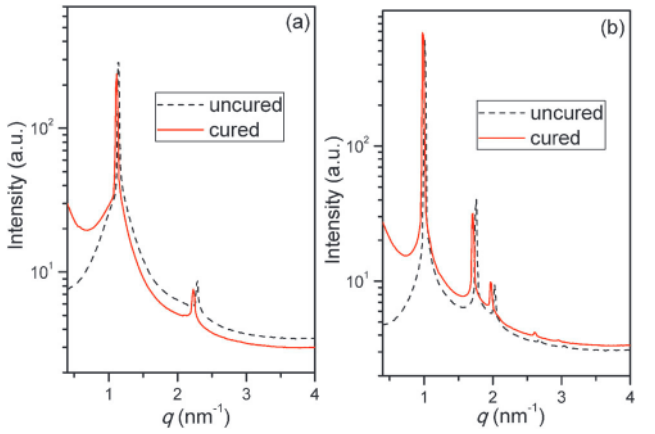

Fig. 9 Representative SAXS patterns for the LLC phases along dilution line F before and after cross-linking: (a) lamellar with 20 wt% water (F20 in Fig. 2); (b) hexagonal with 40 wt% water (F40 in Fig. 2).

Retention of LLC phases after polymerization

As discussed earlier, the lack of thermal stability of LLCs has greatly limited their applications and it is challenging to polymerize LLCs while fully retaining the precursor nanostructure. Polymerizable LLC systems with conventional polymeizable monomers like poly(ethylene glycol) diacrylate (PEGDA) and 1,6-hexanediol diacrylate (HDDA) exhibited disrupted nanostructures due to monomer segregation and phase separation during polymerization.[36] The preservation of LLC nanostructure templates after polymerization of polymerizable MA–PEO–PDMS–PEO–MA was demonstrated by comparison of SAXS patterns and POM images for the samples before and after polymerization, respectively. Two representative samples from lamellar and hexagonal phase regions were intentionally selected for this study. As shown in Fig. 9(a), the SAXS profiles exhibit a ratio between the primary and secondary reflections of 1 : 2 for the sample with 20 wt% water content along dilution line F before polymerization. After polymerization, these SAXS peaks with the relative positions of 1 : 2 were retained, indicating the preservation of lamellar phase during polymerization. Similar results for the hexagonal phase with 40 wt% water content along dilution line F were also observed. As shown in Fig. 9(b), the characteristic peaks for hexagonal phase with relative positions of 1 : 0 3 : 0 4 were retained upon polymerization. Analysis of the SAXS patterns yields essentially equivalent lattice parameters for the LLC phases before and after polymerization. Specifically, lattice parameters were 5.47 nm and 5.65 nm for the lamellar phase and 6.23 nm and 6.38 nm for the hexagonal phase, indicating the retention of nanostructure in these systems after polymerization. However, as indicated by POM (data not shown), dilution of the polymerized LLCs with water resulted in the disappearance of LLC structure, suggesting that internal cross-linking of LLCs did not take place.

POM results further confirm the retention of LLC phases after polymerization. As shown in Fig. 10(a) and (b), after polymerization, the streaked texture for the lamellar phase was preserved without significant loss of birefringence, indicating the lamellar phase was retained after polymerization. The retention of streaked texture for the lamellar phase is comparable to the ternary LLC system with polymerizable poly(ethylene glycol) (PEG), dodecyltrimethylammonium bromide (DTAB), and water.[34] Similar POM results for the retained hexagonal phase with parallel striation texture were shown in Fig. 10(c) and (d). Taken together with the SAXS results in Fig. 9, it can be concluded that polymerization of polymerizable MA–PEO–PDMS–PEO–MA did not alter the nanostructure of the parent LLCs.

Enhanced thermal stability of polymerized LLC

The effect of polymerization on the thermal stability of these LLCs was investigated by SAXS measurement at different temperatures. Fig. 11(a) shows that the SAXS profiles of the sample with 20 wt% water content before polymerization at various temperatures ranging from 25 to 80 1C. At 25 1C, there were two clear scattering peaks with relative positions of 1 : 2, indicating a well-developed lamellar structure. From 25 to 55 1C, the sharpness and intensity of these characteristic SAXS peaks from the lamellar phase decreased. At 60 1C the first primary peak distinctly broadened and the second higher-order peak became difficult to observe. Above 60 1C, a single broad SAXS peak was observed due to the melting of the lamellar phase. Cross-linking of the polymerizable MA–PEO–PDMS–PEO–MA in the lamellar phase clearly enhanced its thermal stability, which was evidenced by the SAXS patterns in Fig. 11(b). The SAXS profiles of polymerized lamellar phase with relative peak positions of 1 : 2 could be observed even up to 80 1C, the highest temperatures tested.

The photopolymerization of hexagonal phase was carried out for Brij 97/water/MA–PEO–PDMS–PEO–MA ternary mixture with 40 wt% water along dilution line F. Fig. 12(a) shows that the SAXS patterns for the mixture before polymerization from 25 to 65 1C. At 25 1C, it exhibits three clear scattering peaks with relative positions of 1 : 0 3 : 0 4 for the hexagonal phase. When the temperature was increased from 30 to 40 1C, the sharpness and intensity of these peaks decreased similarly to those of for

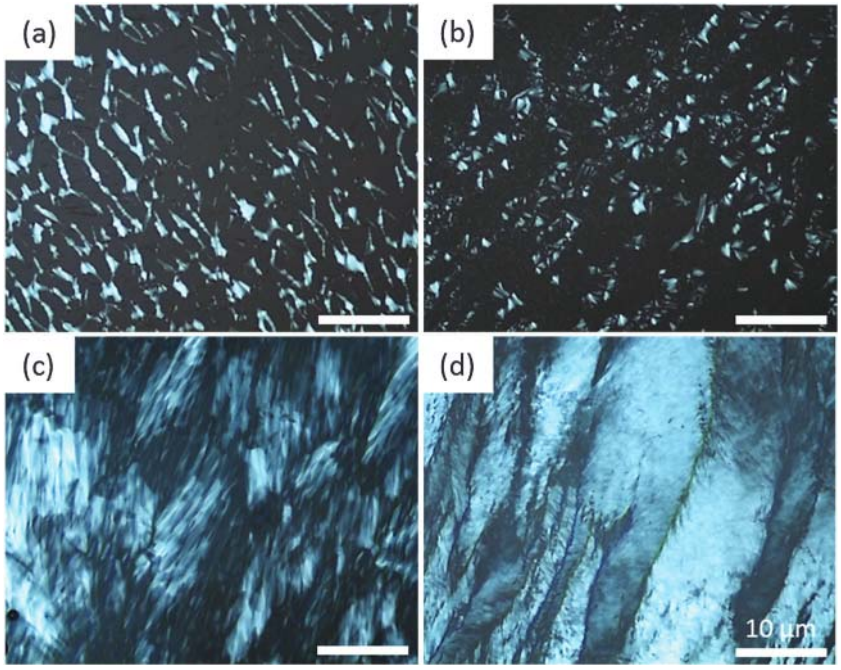

Fig. 10 POM optical textures for the Brij 97/water/MA–PEO–PDMS–PEO–MA ternary system before and after polymerization: (a) F20 before polymerization; (b) F20 after polymerization; (c) F40 before polymerization; (d) F40 after polymerization.

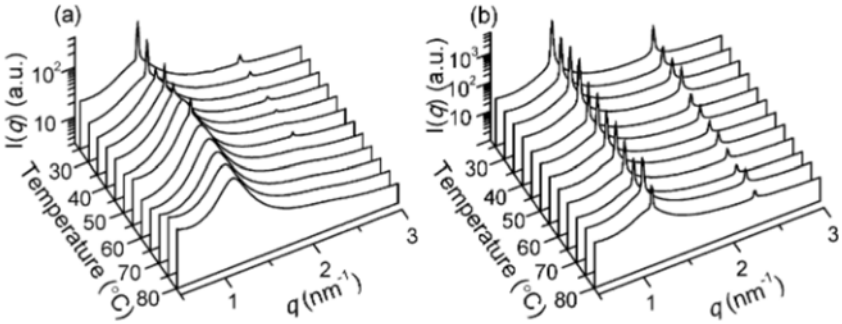

Fig. 11 SAXS patterns plotted as a function of temperature for the formulation along dilution line F with 20 wt% water content (F20 in Fig. 2): (a) before polymerization; (b) after polymerization.

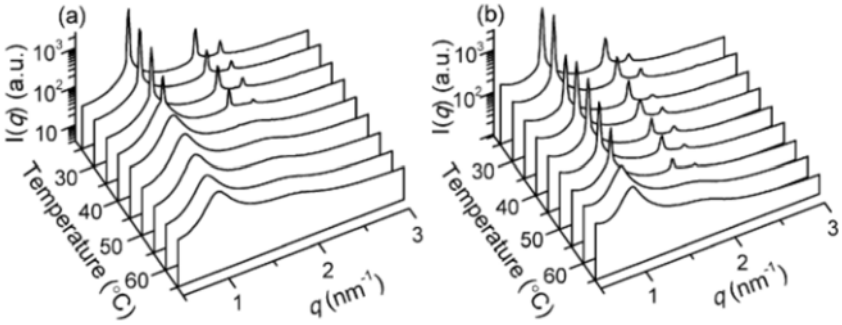

Fig. 12 SAXS patterns plotted as a function of temperature for the formulation along dilution line F with 40 wt% water content (F40 in Fig. 2): (a) before polymerization; (b) after polymerization.

the lamellar phase (Fig. 11(a)). At 45 1C, the SAXS pattern evolved into two distinctly broadened peaks, indicating the melting of hexagonal phase and the onset of micelles. The broader peak was presumably due to the fact that, with increased thermal fluctuations, the closely packed micelles in LLC phase simply break more often and become increasingly

Table 1 Thermal stability of different LLC mesophases before and after polymerization in terms of their melting points with an accuracy of 5 °C was determined by SAXS measurements

Sample/LLCs	Lattice parameters (nm) (before/after)	Composition (wt%)			Melting point (°C)	
		Water	Brij 97	MA–PEO–PDMS–PEO–MA	Before	After
E25/L_a	5.54/5.68	25	37.5	37.5	50	4 80
F25/L_a	5.46/5.61	25	45	30	55	4 80
G25/L_a	5.51/5.64	25	52.5	22.5	60	4 80
F20/L_a	5.47/5.65	20	48	32	55	4 80
F35/H_1	6.01/6.14	35	39	26	45	60
F40/H_1	6.23/6.38	40	36	24	45	60
F45/H_1	6.59/6.72	45	33	22	55	60

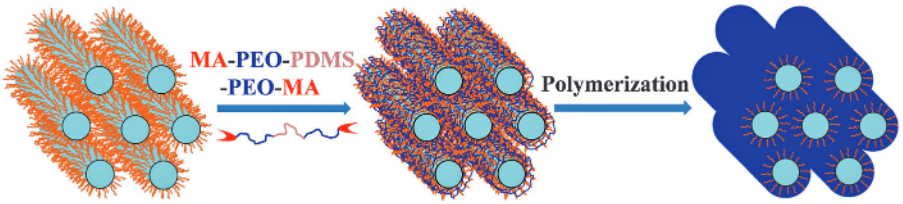

Scheme 2 Schematic illustration of polymerizable surfactant was incorporated into hexagonal phase and the initial structure was retained after polymerization.

shorter until they reach an isotropic micellar state.[46,47] As shown in Fig. 12(b), the clearly improved thermal stability of the hexagonal phase was again indicated by the increased melting point, from 45 to 60 °C after polymerization of the ternary mixture. It is noted that the melting point of the polymerized hexagonal phase was lower than that of lamellar phase. This may be due to the different polymerizable MA–PEO–PDMS–PEO–MA contents in the ternary mixture. For the lamellar phase with 20 wt% water content, the content of polymerizable MA–PEO–PDMS–PEO–MA in the mixture is 32 wt%. The polymerizable content decreases to 24 wt% for the hexagonal phase with 40 wt% water. The higher concentration of polymerizable compound in the lamellar phase resulted in more cross-linked points in the polymerized mixture, thus enabling higher thermal stability of the system after polymerization.

Another possible explanation for the different thermal stability of lamellar and hexagonal phases after polymerization could be due to their different intrinsic interfacial architectures. Compared with highly curved hexagonal phase, non-curved planar lamellar phase makes the polymerizable double bonds more closely aligned, resulting in the polymerized lamellar phase being more stable than the hexagonal phase. It has been reported that polymerization kinetics is closely related to LLC phase geometry and that faster polymerization rates and higher retention of parent LLC phases was observed for a lamellar phase.[27,35] Thermal stability of seven LLC samples with four L_a phases and three H_1 phases before and after polymerization was summarized in Table 1. It can be clearly seen that the melting points of polymerized L_a phases are consistently higher than the polymerised H_1 phases even though the content of polymerizable MA–PEO–PDMS–PEO–MA was lower in the L_a phase (G25, 22.5 wt%), indicating that the intrinsic interfacial architectures of LLCs may play more pronounced role in affecting polymerization efficiency and thermal stability. Finally, a sketch illustrates the role of incorporated polymerizable surfactant and the effect of polymerization on the phase of LLCs was given in Scheme 2.

Conclusions

This work presents a facile method to prepare thermally stable and mechanically robust LLCs by simply incorporating a polymerizable amphiphile. The polymerizable MA–PEO–PDMS–PEO–MA was synthesized and incorporated into the binary Brij 97/water LLC system. The phase behaviour of the ternary mixture of Brij 97/water/MA–PEO–PDMS–PEO–MA was intensively studied by POM and SAXS and two LLC phase regions including lamellar and hexagonal were identified. SAXS measurements indicated that all of the parent LLC nanostructures reported here can be retained after polymerization of MA–PEO–PDMS–PEO–MA within the lamellar and hexagonal phases respectively. Significant improvement of mechanical properties was observed and two orders of magnitude increase of storage modulus and viscosity were obtained after polymerization of the lamellar phase structure. Improved thermal stabilities of polymerized LLCs were observed. However, the degree of induced stability varied according to different phase behaviour of the precursor LLC templates. The higher concentration of polymerizable MA–PEO–PDMS–PEO–MA in the lamellar phase resulted in more cross-linked points in the polymerized mixture, thus enabling higher thermal stability of the system after polymerization. The ability to enhance the thermal stability and mechanical strength of LLCs simply by adding a polymerizable amphiphile has been shown to be a simple and effective way to prepare robust nanomaterials with well-defined periodic structures.

Acknowledgements

SAXS/WAXS research was undertaken at the Australian Synchrotron, Victoria, Australia and the authors thank Dr Nigel Kirby

for his assistance. S.P. gratefully acknowledges Deakin University and CSIRO for provision of a collaborative PhD scholarship.

References

1 D. L. Gin, W. Q. Gu, B. A. Pindzola and W. J. Zhou, Acc. Chem. Res., 2001, 34, 973–980.
2 M. A. DePierro and C. A. Guymon, Macromolecules, 2006, 39, 617–626.
3 D. L. Gin, J. E. Bara, R. D. Noble and B. J. Elliott, Macromol. Rapid Commun., 2008, 29, 367–389.
4 J. D. Clapper and C. A. Guymon, Adv. Mater., 2006, 18, 1575.
5 M. A. DePierro, K. G. Carpenter and C. A. Guymon, Chem. Mater., 2006, 18, 5609–5617.
6 D. L. Gin, X. Lu, P. R. Nemade, C. S. Pecinovsky, Y. Xu and M. Zhou, Adv. Funct. Mater., 2006, 16, 865–878.
7 B. S. Forney, C. Baguenard and C. A. Guymon, Soft Matter, 2013, 9, 7458–7467.
8 D. T. McCormick, K. D. Stovall and C. A. Guymon, Macromolecules, 2003, 36, 6549–6558.
9 S. Peng, Q. Guo, T. C. Hughes and P. G. Hartley, Langmuir, 2014, 30, 866–872.
10 R. Yang, S. Peng and T. C. Hughes, Soft Matter, 2014, 10, 2188–2196.
11 S. Peng, P. G. Hartley, T. C. Hughes and Q. Guo, Soft Matter, 2012, 8, 10493–10501.
12 Z. F. Chen, T. L. Greaves, R. A. Caruso and C. J. Drummond, J. Mater. Chem., 2012, 22, 10069–10076.
13 S. D. Shen, A. E. Garcia-Bennett, Z. Liu, Q. Y. Lu, Y. F. Shi, Y. Yan, C. Z. Yu, W. C. Liu, Y. Cai, O. Terasaki and D. Y. Zhao, J. Am. Chem. Soc., 2005, 127, 6780–6787.
14 L. L. Cheng, Y. Y. Luk, C. J. Murphy, B. A. Israel and N. L. Abbott, Biomaterials, 2005, 26, 7173–7182.
15 C. J. Drummond and C. Fong, Curr. Opin. Colloid Interface Sci., 1999, 4, 449–456.
16 C. Y. Guo, J. Wang, F. L. Cao, R. J. Lee and G. X. Zhai, Drug Discovery Today, 2010, 15, 1032–1040.
17 X. Mulet, B. J. Boyd and C. J. Drummond, J. Colloid Interface Sci., 2013, 393, 1–20.
18 B. W. Muir, D. P. Acharya, D. F. Kennedy, X. Mulet, R. A. Evans, S. M. Pereira, K. L. Wark, B. J. Boyd, T. H. Nguyen, T. M. Hinton, L. J. Waddington, N. Kirby, D. K. Wright, H. X. Wang, G. E. Egan and B. A. Moffat, Biomaterials, 2012, 33, 2723–2733.
19 M. J. Moghaddam, L. de Campo, L. J. Waddington and C. J. Drummond, Soft Matter, 2010, 6, 5915–5929.
20 M. Caffrey, Curr. Opin. Struct. Biol., 2000, 10, 486–497.
21 M. Caffrey, Biochem. Soc. Trans., 2011, 39, 725–732.
22 C. E. Conn, C. Darmanin, X. Mulet, A. Hawley and C. J. Drummond, Soft Matter, 2012, 8, 6884–6896.
23 S. A. Miller, J. H. Ding and D. L. Gin, Curr. Opin. Colloid Interface Sci., 1999, 4, 338–347.
24 H. Ringsdorf, B. Schlarb and J. Venzmer, Angew. Chem., Int. Ed., 1988, 27, 113–158.
25 A. Sellinger, P. M. Weiss, A. Nguyen, Y. F. Lu, R. A. Assink, W. L. Gong and C. J. Brinker, Nature, 1998, 394, 256–260.
26 J. M. Schnur, R. Price, P. Schoen, P. Yager, J. M. Calvert, J. Georger and A. Singh, Thin Solid Films, 1987, 152, 181–206.
27 C. L. Lester and C. A. Guymon, Polymer, 2002, 43, 3707–3715.
28 L. Sievens-Figueroa and C. A. Guymon, Chem. Mater., 2009, 21, 1060–1068.
29 B. Soberats, E. Uchida, M. Yoshio, J. Kagimoto, H. Ohno and T. Kato, J. Am. Chem. Soc., 2014, 136, 9552–9555.
30 B. S. Forney and C. A. Guymon, Macromol. Rapid Commun., 2011, 32, 765–769.
31 R. Yang, S. Peng, W. Wan and T. C. Hughes, J. Mater. Chem. C, 2014, 2, 9122–9131.
32 S. Peng, Q. Guo, T. C. Hughes and P. G. Hartley, Macromolecules, 2011, 44, 3007–3015.
33 L. Sievens-Figueroa and C. A. Guymon, Macromolecules, 2009, 42, 9243–9250.
34 C. L. Lester, C. D. Colson and C. A. Guymon, Macromolecules, 2001, 34, 4430–4438.
35 C. L. Lester and C. A. Guymon, Macromolecules, 2000, 33, 5448–5454.
36 B. S. Forney and C. A. Guymon, Macromolecules, 2010, 43, 8502–8510.
37 R. L. Kerr, S. A. Miller, R. K. Shoemaker, B. J. Elliott and D. L. Gin, J. Am. Chem. Soc., 2009, 131, 15972.
38 M. A. Reppy, D. H. Gray, B. A. Pindzola, J. L. Smithers and D. L. Gin, J. Am. Chem. Soc., 2001, 123, 363–371.
39 B. P. Hoag and D. L. Gin, Macromolecules, 2000, 33, 8549–8558.
40 S. Peng, Q. Guo, P. G. Hartley and T. C. Hughes, J. Mater. Chem. C, 2014, 2, 8303–8312.
41 J. M. Seddon, A. M. Squires, C. E. Conn, O. Ces, A. J. Heron, X. Mulet, G. C. Shearman and R. H. Templer, Philos. Trans. R. Soc., A, 2006, 364, 2635–2655.
42 J. L. Yang and G. Wegner, Macromolecules, 1992, 25, 1786–1790.
43 Z. F. Chen, T. L. Greaves, C. Fong, R. A. Caruso and C. J. Drummond, Phys. Chem. Chem. Phys., 2012, 14, 3825–3836.
44 L. H. Chen, G. S. Zhu, D. L. Zhang, H. Zhao, M. Y. Guo, S. B. Wei and S. L. Qiu, J. Mater. Chem., 2009, 19, 2013–2017.
45 K. S. Anseth, C. N. Bowman and L. BrannonPeppas, Biomaterials, 1996, 17, 1647–1657.
46 J. F. Berret, J. Appell and G. Porte, Langmuir, 1993, 9, 2851–2854.
47 M. E. Cates, J. Phys. Chem., 1990, 94, 371–375.

